Humid heatwaves are controlled by daily rainfall variability

Lawrence Jackson

l.s.jackson@leeds.ac.uk

University of Leeds https://orcid.org/0000-0001-8143-2777

Cathryn Birch

University of Leeds https://orcid.org/0000-0001-9384-2810

Guillaume Chagnaud

UK Centre for Ecology and Hydrology

John Marsham

University of Leeds https://orcid.org/0000-0003-3219-8472

Christopher Taylor

UK Centre for Ecology and Hydrology https://orcid.org/0000-0002-0120-3198

Article

Keywords:

Posted Date: September 20th, 2024

DOI: https://doi.org/10.21203/rs.3.rs-5037159/v1

Additional Declarations: There is **NO** Competing Interest.

Abstract

Humid heatwaves are a growing risk to human and animal health, especially in tropical regions. While there is established research on dry-bulb temperature heatwaves, greater understanding of the meteorological drivers is urgently needed. In this study, we find that recent rainfall is a key control on the occurrence of humid heatwaves and its effect is regulated by the energy- or moisture-limited state of the land surface. In moisture-limited environments, heatwaves are likely during, or immediately after, enhanced rainfall. In energy-limited environments, heatwaves are likely after suppression of rainfall for two days or longer. The nature of the threat to health from heat stress varies by environment. It depends on local adaptation to temperature or humidity extremes, as well as vulnerability to absolute or anomalous extremes. Adaptation and early warning will benefit from this new understanding of humid heatwave drivers, which shows the possibility of predicting events using satellite-derived rainfall and surface moisture data.

Introduction

Periods of combined high temperature and humidity result in heat stress, which can have a significant impact on human and animal health[1] and restrict economic activity, such as outdoor work[2]. Studies on human physiological responses to humid heat extremes suggest a potential limit to human adaptability to such conditions. After a few hours of exposure to wet-bulb temperature (Twb) of 35°C, effective thermoregulation may become impossible[3]. Recent empirical studies suggest that health impacts occur at around 31°C for young, healthy individuals[4], and likely at much lower values for vulnerable groups such as the very young and the elderly. The focus of this study is on the physical processes involved in the occurrence of humid heatwaves, with particular attention to the role of rainfall variability.

Humid heat extremes have intensified since 1979[5,6] and become more frequent[5,7]. Some regions in the subtropics, such as coastal areas around the Persian Gulf, have already experienced short-lived Twb extremes above 35°C[5,8]. Climate change is driving the occurrence of more extreme humid heat events, as seen in South and Southeast Asia in April 2023[9]. Most importantly, humid heat stress is projected to become more severe under future climate change[10,11,1,12–16].

Along with an increased awareness of the risks posed by humid heatwaves there has been a growing focus on their underlying processes. In regions such as the southern Persian Gulf, north-central Pakistan, eastern South Asia, and the western Amazon, strong surface evaporation and the inhibition of convection by atmospheric stability play a key role in the occurrence of humid heat extremes[17]. A study using a pan-Africa convection permitting climate model[18] found that humid heat is often associated with rainfall, with approximately one-third of humid heatwaves starting on wet days. In addition to rainfall, other factors exerting a control over humid heatwaves in all but the most humid regions of Africa include increases in cloud cover, surface longwave radiation and surface evaporation. However, in highly humid

regions such as the Congo Basin, factors regulating dry-bulb temperature are more significant than rainfall[18].

Unlike dry heatwaves, extreme Twb events often occur during the monsoon season rather than prior to it, and the association between rainfall and humid heat varies with the local near-surface moisture climatology[19]. In parts of South Asia with relatively low humidity, Twb extremes are more likely during periods of enhanced rainfall, whereas Twb extremes are more likely during suppressed rainfall in regions of higher humidity[19]. In the arid and semi-arid regions of the global tropics and subtropics, light rain sustains surface evaporation and is associated with more frequent and more intense wet-bulb globe temperature extremes during the hottest four months of the year[20]. Irrigation has been shown to be important for humid heat extremes in India[21] and the northern plains of China[22] but there is no consensus on the nature of its control[23,24] partly due to different regional impacts of irrigation on moisture transport[25]. Land-atmosphere feedbacks intensify and help the propagation of dry heatwaves[26] and increasing ecosystem water limitations are linked with intensified future dry heat extremes[27]. A widespread positive correlation between Twb and soil moisture[28] suggests that land-atmosphere feedbacks also play a key role in humid heat extremes. Much of the existing research on humid heat processes, however, is limited to regional scale mechanisms and the understanding of underlying processes remains poorly understood[1,16].

We have two aims for this study. Our first aim is to characterise the relationship between occurrences of humid heatwaves and rainfall over land across the global tropics and subtropics. Our second aim is to test the hypothesis promulgated by Ivanovich et al.[19] and Zhang et al.[20] that rainfall regulates humid heat extremes through surface moisture flux processes that vary between energy- and moisture-limited environments[29,30]. Importantly, our study focuses on the global tropics and subtropics whereas Ivanovich et al.[19] focus on South Asia. Additionally, our study addresses both the promotion and suppression of humid heat extremes, whereas Zhang et al.[20] focus more on the enhancement of extremes.

In this study, we prepare a dataset of humid heatwaves using ERA5 data and identify distinct heatwave events using a time-space connected components method that has previously been used in the identification of heatwaves[31,32]. We use the local 95th percentile of daily mean Twb, with an absolute minimum of 24°C, to capture humid heat events that are both high for the locality and at or close to the intensity that poses a threat to human health. We prepare a dataset of enhanced and suppressed rainfall days using GPM-IMERG data and assess the significance of the relationship between humid heatwaves and rainfall in years 2001 to 2022. At the time of each heatwave, we classify the surface environments as energy- or moisture-limited using the Ecosystem Limitation Index[33], an index of surface energy- and moisture-limitation that has previously been used in the study of dry heat extremes[27].

We use daily mean Twb as our primary measure of humid heat. It combines both temperature and humidity and has similar thermodynamic properties to equivalent potential temperature (θe), making it

robust for analysis on regional scales[34]. Furthermore, Twb is relevant to human heat stress. It provides an upper temperature limit for healthy, well-acclimatised human beings who have access to drinking water, shade, and a strong breeze[1].

We find that there is a statistically significant relationship between humid heatwaves and daily rainfall across tropical land areas. Exploring the extent to which this relationship is explained by energy- or moisture-limitations shows the key role of surface evaporation of recent rainfall in many regions of the tropics and subtropics.

Results

Humid heatwaves and seasonal rainfall

The occurrence of humid heatwaves is widespread across the global tropics and subtropics (Fig. 1A). These heatwaves occur in monsoon regions such as West Africa, India, East China, and north Australia, and in equatorial regions such as the Amazon, the Congo basin, and the Maritime Continent. Most of these regions experience 1–2 heatwaves per year. In general, the frequency of occurrence decreases sharply at the northern and southern extent of regional monsoons due to climatologically low humidity (e.g. West Africa, Australia) and in regions at high elevation due to lower dry-bulb temperatures at altitude (e.g., the Himalayan region in India and inland East Africa). The heatwaves are relatively small in size. The minimum size of the heatwaves is approximately 1,900 km^2 (by definition), while the median size is approximately 4,400 km^2.

The mean duration of humid heatwaves is typically between 3 and 12 days (Fig. 1B). Regions with the longest heatwave durations include eastern Brazil and the equatorial east coast of Africa. In contrast, the West African Sahel experiences relatively short duration heatwaves (3–6 days). Heatwave intensity, represented by the 90th percentile of daily mean Twb on heatwave days, typically ranges between 24°C and 27°C (Fig. 1C). Regions with the most intense heatwaves include the Red Sea and Persian Gulf coastlines, Pakistan, northern India and Bangladesh, and northeast China, where the daily mean Twb 90th percentile ranges between 28°C and 31°C. Daily maximum Twb can be much higher[18,35].

Humid heatwaves and regional rainfall exhibit a strong seasonal cycle (Figs. 1D and 1E). Over the western and central regions of the Amazon basin, heatwaves most frequently occur during October-November, marking the transition from the dry to wet season. In equatorial regions (10°S − 10°N), humid heatwaves occur at the time of the seasonal migration of the tropical rain-belt, particularly in March-May over eastern South America, Africa, and western Maritime Continent. Regions such as India, Southeast Asia, East and West Africa, and North Australia are farther from the equator and experience strong monsoon seasons (e.g., peak rainfall occurs in July-August over much of India). In these regions, humid heatwave occurrence appears to synchronise with monsoon seasons.

To show the relationship between humid heatwaves and seasonal rainfall at the monthly timescale, Fig. 1F shows the number of months separating the seasons of peak rainfall and peak humid heat (i.e., the difference between Figs. 1E and 1D). The seasons of rainfall and humid heat are closely synchronised in regions beyond latitudes 10°S – 10°N that have strong seasonal monsoons. These are regions shaded orange, cream, or light blue in Fig. 1F (e.g., West African Sahel). However, it is important to note that this association between seasonal rainfall and humid heat does not establish a causal relationship between the two phenomena. Furthermore, there are many regions exposed to humid heat in which peak seasonal rainfall and humid heat do not coincide. These regions, where heatwaves can occur before or after seasonal rainfall, are shaded purple in Fig. 1F.

Rainfall variability as a driver of humid heatwave occurrence

In the previous section, we established a link between the timing of humid heatwaves and of rainfall at the seasonal timescale. As a step towards a process-based understanding, we now examine the relationship on the daily timescale in each grid cell using months in which at least one humid heatwave occurred. We categorised each day into one of four groups based on whether rainfall was higher or lower than a minimum threshold of 5 mm/day in a two-day window, and whether a heatwave started or not. The groups with higher rainfall ("High_Rain") include days when rainfall exceeds 5mm/day on that day, or the previous day, or on both days. The groups with lower rainfall ("Low_Rain") include days when rainfall does not exceed 5mm/day on both that day and the previous day. We used counts of the number of days in each group to calculate empirical probabilities for heatwaves starting on High_Rain days or Low_Rain days (see Methods for more details).

In Fig. 2A, we map the relative risk (the ratio of the two probabilities) in those grid cells where there is a statistically significant difference between the probabilities. Blue shades represent grid cells where heatwaves are more likely on High_Rain days, and red shades represent grid cells where heatwaves are more likely on Low_Rain days. There is a clear geographic pattern which resembles the Köppen-Geiger classification of climate zones[36]; humid heatwaves are more likely to occur on High_Rain days in arid regions (Köppen-Geiger Zone B). In contrast, humid heatwaves are more likely to occur on Low_Rain days in tropical and equatorial regions (Köppen-Geiger Zone A).

To examine the role of surface energy- and moisture-limitations in modulating the relationship between rainfall and humid heat, we calculated the Ecosystem Limitation Index[33] (ELI) daily for each grid cell. The ELI is calculated as the difference between the correlations of surface latent heat flux with near-surface soil moisture and downwelling shortwave (SW) radiation at the surface using surface variables from ERA5 (see Methods). Positive values for the ELI mean that soil moisture exerts a stronger control on surface evaporation than downwelling surface SW radiation, signifying that moisture-limitation is greater than the energy-limitation. Hereafter, we refer to this as moisture-limitation. In contrast, negative values indicate greater energy-limitation than moisture-limitation, which hereafter we refer to simply as energy-limitation. In Fig. 2B, the ELI shown is a heatwave-composite mean of values taken two days before the start of humid heatwaves. This ELI, therefore, represents surface energy- and moisture-limitation

immediately before and at the start of humid heatwaves and is not necessarily indicative of the local seasonal climatology.

The scatter plot of grid cell data in Fig. 2C shows that humid heatwaves fall into one of four rainfall-ELI regimes. Regime 0, in which heatwaves occur in moisture-limited environments and are more likely on Low_Rain days, is relatively rare (0.1% grid cells, red shading). Its grid cells have relatively small ELI values (median 0.27) which could potentially result from noise in other regimes. Therefore, Regime 0 is not examined further, along with grid cells that are not statistically significant (66% of the grid cells, white shading).

As suggested by Figs. 2A and 2B, heatwaves occurring in moisture-limited environments generally occur on High_Rain days (Regime 1) and account for 7% of grid cells (Figs. 2C and 2D, dark blue shading). Heatwaves occurring in energy-limited environments generally occur on Low_Rain days (Regime 2) and account for 22% of the grid cells (Figs. 2C and 2D, orange shading). For grid cells with moderate relative risk values (i.e., relative risk < 10), there is a strong linear relationship between relative risk and ELI (Pearson correlation coefficient + 0.74). Grid cells on the right-hand side of Fig. 2C with relative risk values > 10 (i.e., where Eq. (3) applies; see Methods) have a mean ELI of + 0.92 ± 0.01 (± 1 standard error) and are clearly moisture-limited. Similarly, grid cells on the left-hand side of Fig. 2C with relative risk values > 10 (i.e., where Eq. (4) applies; see Methods) have a mean ELI of -1.14 ± 0.02 and are clearly energy-limited.

There are also regions where the role of rainfall is more subtle (Regime 3). In parts of western India, Mozambique, and North Australia, the local environment is energy-limited according to the ELI, yet heatwaves are more likely on High_Rain days (Figs. 2C and 2D, light blue shading). This apparent contradiction is explained in the next section, where we show that surface evaporation in Regime 3 is sensitive to both energy- and moisture-limitations.

Contributions of temperature and humidity to humid heatwaves

Figure 3 shows composite time series centred on the first day of each heatwave for Twb, 2m temperature, and specific humidity. Regions in Regime 1 are climatologically hot and dry, with relatively modest levels of Twb prior to the heatwaves, consistent with the moisture-limited nature of Regime 1 (Fig. 2C). Anomalies in temperature and humidity grow strongly starting two days before the heatwaves, coinciding with days of High_Rain immediately before and at the start of the heatwaves. In Regime 1, humid heatwaves result from large positive humidity anomalies, partly offset by negative 2m temperature anomalies (approximately − 2°C).

Regime 2 is energy-limited (Fig. 2C) and is climatologically cooler and more humid than Regime 1. Anomalies in temperature and humidity grow during the first two days of the heatwaves following two days of Low_Rain. Unlike Regime 1, humid heatwaves in Regime 2 result from positive anomalies in both 2m temperature and specific humidity. Although heatwaves have the largest absolute Twb in Regime 2, the temperature and humidity anomalies are smaller than those in Regime 1.

Regime 3 is climatologically similar to Regime 2 although slightly hotter and less humid. In contrast to Regime 2, heatwaves in Regime 3 primarily result from positive specific humidity anomalies. There is a slight increase in 2m temperatures from day − 1 to day 1, although the anomalies remain close to climatology.

The controlling role of surface energy- and moisture-limitations

To elucidate the mechanisms underpinning each heatwave regime, Fig. 4 presents composite time series centred on the first day of each heatwave for several surface and atmospheric variables.

Rainfall anomalies on day − 1 and day 0 differ between the regimes by design. Differences in anomalies on days − 7 to -2 and days 1 to 7, however, provide insight into the role of rainfall variability in the occurrence of humid heatwaves. In Regime 1 (moisture-limited), daily mean rainfall is relatively low. The rainfall anomaly increases strongly in the two days before the heatwave, and is enhanced just prior to the start of the heatwave (day − 1). For Regimes 2 and 3 (energy-limited), daily mean rainfall is greater three or more days before the start of a heatwave. In Regime 2, rainfall decreases sharply two days before a heatwave, it is suppressed at the start of a heatwave, and returns to its daily climatology over the next three days. In Regime 3, positive rainfall anomalies occur in the run up to a heatwave (days − 6 to -1). Rainfall decreases to its climatology at the start of a heatwave followed by a peak in rainfall three days later when the heatwaves start to dissipate.

In summary, rainfall variability at the start of a humid heatwave can be characterised as enhanced (Regime 1), suppressed (Regime 2), or decreased (Regime 3).

Regime 1 (ELI moisture-limited and enhanced rainfall)

Prior to rainfall, the environment in these regions is relatively dry characterised by low rainfall, low total column water vapour (TCWV), low soil moisture, and a relatively deep boundary layer (Fig. 4). Rainfall immediately before and/or during the first days of a heatwave, increases soil moisture and promotes humidification of the boundary layer through a strong increase in surface latent heat flux. Humidity may also be enhanced aloft by moisture convergence associated with the rain-bearing storms. The overall increase in surface latent heat flux is accompanied by a decrease in surface sensible heat flux, which is characteristic of moisture-limited environments. This decrease in surface sensible heat flux reduces the depth of the boundary layer, concentrating humidity near the surface. The increase in atmospheric humidity enhances downwelling longwave radiation at the surface, although this increase in surface radiation is more than offset by attenuation of downwelling SW radiation due to increased cloud cover associated with the storms. The associated changes in upwelling surface radiation fluxes are shown in Figure S6.

Regime 2 (ELI energy-limited and suppressed rainfall)

The environment in these regions is wetter and the supply of energy and moisture from the surface to the near-surface air differs from regions that are moisture-limited. Prior to a heatwave, rainfall and TCWV

are greater than in the moisture-limited regime, and wetter soils support greater latent heat fluxes at the surface. Cloud cover associated with the rainfall prior to heatwaves attenuates downwelling SW radiation at the surface.

The humid heatwaves in these regions are associated with suppressed rainfall from the day before the start of a heatwave to two days after the start of the heatwave although the near-surface soil remains moist and the atmosphere humid. Positive anomalies in downwelling SW radiation, which exceed 25 Wm^{-2}, promote increases in both surface latent and sensible heat fluxes. These are changes characteristic of energy-limited environments, due to climatologically wetter soils.

Regime 3 (ELI energy-limited and decreased rainfall)

Prior to the onset of humid heatwaves (day − 7), the environment in these regions resembles that of Regime 2 in terms of rainfall, TCWV, and downwelling SW radiation at the surface. In Regime 3, however, the surface is drier with less near-surface soil moisture.

The critical difference between Regimes 2 and 3 is the response of surface latent heat fluxes to changes in surface moisture and energy, as indicated by the correlations between these variables (Table 1). Over the 15 days centred on the start of the humid heatwaves, Regime 3 has positive correlations for surface latent heat flux anomalies with both soil moisture anomalies (+ 0.88) and downwelling SW radiation anomalies (+ 0.54). In contrast, Regime 2 has a negative correlation between surface latent heat anomalies and soil moisture anomalies (-0.76) and a positive correlation between surface latent heat anomalies and downwelling SW radiation anomalies (+ 0.99). For comparison, Regime 1 (moisture-limited) has correlations of + 0.96 between surface latent heat flux anomalies and soil moisture anomalies and − 0.47 between surface latent heat flux anomalies and downwelling SW radiation anomalies.

Table 1
Correlations of anomalies in surface latent heat flux, soil moisture, and downwelling SW radiation for each regime.

Regime	Correlation of surface latent heat flux anomalies with	
	Soil moisture anomalies	Downwelling SW radiation
2	+ 0.96	-0.47
3	-0.76	+ 0.99
4	+ 0.88	+ 0.54

In Regime 3, prior to the onset of a humid heatwave, surface evaporation and Twb are constrained by surface energy and moisture availability. Rainfall prior to a humid heatwave (days − 7 to -2) supplies the necessary surface moisture, while a decrease in rainfall around the start of a heatwave (days − 1 and 0) is accompanied by an increase in downwelling SW radiation which increases surface energy. Together, these changes overcome the initial constraints on surface energy and moisture leading to an increase in

surface latent heat flux. This, in turn, raises near-surface humidity and Twb. These changes are reinforced by a shallower boundary layer resulting from weaker surface sensible heat fluxes.

In summary, although Regime 3 is energy-limited according to the ELI, both energy- and moisture-limitations actually influence surface evaporation in this regime.

The most extreme humid heatwaves

To examine the most extreme humid heatwaves, we focus on events in each grid cell that have the highest 10% of Twb (Fig. 5). Each grid cell is allocated to the same regime as used for all heatwave events. Conditions during extreme heatwaves in each regime (solid circles) have a wide distribution of temperature and humidity, with substantial overlap between the three regimes (shading). Daily mean Twb during the most extreme events is between 27°C and 28°C in all three regimes. Heat Index[37] (HI) classifications of “Extreme Caution” (HI > ~ 33°C) and “Danger” (HI > ~ 39.5°C) are common in all regimes, although the very highest Twb and HI values occur in Regime 2. The mean maximum daily Twb conditions averaged over all humid heatwaves (crosses) are also similar across the three regimes, ranging from 25°C to 26°C and HI 33°C to 35°C.

Despite the similar conditions experienced during extreme humid heatwaves across the three regimes, the climatological humidity and temperature and their change in the build up to events are very different. Locations within Regime 1 (moisture-limited) are climatologically hot and arid, with a climatological mean Twb during the heatwave season of 22°C. A large increase in humidity is required for a humid heatwave to occur, and in the most extreme events much of this occurs more than 7 days before the event. Locations within Regime 2 (energy-limited) are climatologically more humid, cooler in temperature, with a climatological mean Twb between 24°C and 25°C (during the heatwave season). A large increase in temperature is required for a humid heatwave to occur, and in the most extreme events much of this occurs more than 7 days before the event.

Although the humid heat extremes are similar across the three regimes, the nature of the threat to human health from heat stress varies by regime. The threat depends on whether local populations are better adapted to temperature or humidity extremes, and whether they are more vulnerable to absolute or anomalous extremes.

Discussion

Daily rainfall variability strongly controls humid heatwaves across the global tropics and subtropics in our analysis of ERA5 reanalysis and GPM-IMERG rainfall data. The response of humid heat to rainfall changes is modulated by the sensitivity of surface evaporation to soil moisture levels and downwelling SW radiation at the surface. In Regime 1, the surface environment is moisture-limited and humid heatwaves are more likely immediately after enhanced rainfall. In Regime 2, the surface environment is energy-limited and humid heatwaves are more likely during suppressed rainfall. In Regime 3, surface evaporation is sensitive to both downwelling SW radiation and soil moisture levels, making humid

heatwaves more likely during decreased but sustained rainfall. Regime 0, characterised by moisture-limited conditions where heatwaves are more likely after low rainfall, is not explored in detail. It occurs in few grid cells, which have relatively low values for both relative risk and ELI.

In our assessment of statistical significance for the relationship between humid heatwaves and rainfall, 66% of the grid cells are found to be non-significant. Including these grid cells in our analysis of processes has little impact on the results. In Figs. 3 and 4, their inclusion makes the results for Regimes 2 and 3 more similar (Figures S1 and S2). For Regime 1, the magnitude of the anomalies decreases slightly, likely due to a weaker signal-to-noise ratio in the non-significant grid cells. Additionally, in regions such as the West African Sahel, where there is a pronounced seasonal transition from a hot, dry environment to a warm, rainy environment, a seasonal change from Regime 2 (hot and dry) to Regime 3 (rainy) may occur. We conclude that our findings likely extend over much of the white shaded regions in Fig. 2D, although a logical next step would be to extend the analysis to sub-seasonal time scales in the transition regions.

To test our findings that surface energy- and moisture-limitations modulate the relationship between rainfall and humid heat, we defined a wet-bulb temperature energy-moisture limitation index (TwbLI). This index is analogous to the ELI but instead of using surface latent heat flux anomalies, we use Twb anomalies in the calculation of TwbLI (see Methods). The heatwave-rainfall regimes identified using TwbLI (Figure S3D) resemble those found using ELI (Fig. 2D), particularly for the moisture-limited Regime 1 and the energy-limited Regime 2. Moreover, to first order, there is a strong correlation between the spatial distributions of ELI (Fig. 2B) and TwbLI (Figure S3B) and the spatial distribution of Köppen-Geiger climate zones, particularly for zones A and B. With a projected future shift from energy- to moisture-limitation[33], rainfall variability could play an increasingly important role in future occurrences of humid heatwaves.

We tested the sensitivity of our results to changes in several key assumptions. Similar results were obtained with a 1 mm/day rainfall threshold, where 43% of land grid cells with heatwaves are significant, compared to 45% for the 5 mm/day threshold (Figure S4A). Defining rainy days as days of light rain (i.e. 1–10 mm/day) also produced similar results except the relative risk is weaker for heatwaves on light-rain days (Figure S4B). Excluding days of heavier rainfall weakened the relative risk results in all regions (Figures S3C,D), suggesting heavy rainfall days (and potentially subsequent flooding) may be important for humid heat risk[38]. We also found similar results using ERA5 rainfall for years from 1993 to 2022 instead of GPM-IMERG (Figure S5A). A threshold of 5 mm/day for enhanced rainfall days produced the clearest results for the relative risk of heatwaves occurring on High_Rain versus Low_Rain days and is physically relevant as a reasonable initial estimate of potential evaporation in the tropics.

We used a minimum threshold of 24°C Twb for humid days to identify a sufficiently large number of heatwave events to support robust statistical analysis. Repeating our relative risk analysis using a minimum threshold of 26°C Twb, a level above which vulnerable individuals can be significantly affected by heat stress[39], yielded a consistent spatial pattern of relative risk albeit with substantially reduced

numbers of statistically significant grid cells due to the smaller numbers of heatwave events (Figure S5B).

While Twb is an appropriate measure for humid heat, it has its limitations for assessing human heat stress. It does not fully incorporate the full range of human physiological responses to humid heat and provides a temperature threshold based on conditions ideal for maximal cooling through evaporation. Although an assessment of human heat stress is beyond the scope of this study, we recalculated relative risk using the Heat Index (Figure S5C) and also 2m dry-bulb temperature (Figure S5D). In energy-limited regions where heatwaves are more likely to follow suppressed rainfall, we obtain similar but more strongly significant results using the Heat Index or 2m dry-bulb temperature. In contrast, in moisture-limited regions the strength of the relationship between heatwaves and rainfall is much weaker. This supports our choice of Twb for this study and highlights differences in the sensitivity of different heat stress measures to humidity[40,24,19].

Our results focus on the daily timescale, and an obvious next step would be to extend the analysis to hourly time scales. Extreme humid heat events can be short-lived, and processes at the diurnal timescale such as land-sea breezes, low-level moisture bearing monsoon winds, and moist convection are likely of varying importance across locations in the three regimes identified in this study. A better understanding of humid heatwaves at the sub-daily timescale would inform near-real-time prediction. Future studies could focus on the more slowly evolving, longer timescale atmospheric processes such as ENSO that precondition the local environment for the subsequent development of humid heatwaves. Finally, projected changes in future rainfall patterns[41] and future shifts from energy- to moisture-limited environments[33,27] highlight that the response of humid heatwaves to climate change is likely to be complex at the regional scale.

Our findings are a key step towards greater understanding of the meteorological processes underpinning humid heatwaves at the regional scale. They will be valuable in the evaluation of weather and climate models, will aid the use and interpretation of climate model projections, and ultimately inform the design of much needed early warning systems for humid heat extremes. In particular, the key role of rainfall immediately preceding humid heatwaves suggests that satellite observations of rain and soil moisture could enhance monitoring and early warning systems.

Methods

ERA5 data

We use data from the European Centre for Medium-Range Weather Forecasts (ECMWF) fifth generation reanalysis (ERA5)[42,43]. We use hourly data on the native ERA5 spatial grid (resolution of 0.25° × 0.25°). We exclude February 29th from leap years so that each year has 365 days in our study. All analysis is based on daily means calculated using hourly data based on 0–24 UTC days. We use data for years

1993 to 2022 for Fig. 1 and data for years 2001 to 2022 for Figs. 2–5 (for consistency with GPM-IMERG data).

GPM-IMERG data

We use the daily Integrated Multi-satellitE Retrievals for GPM (IMERG) satellite retrievals of rainfall[44] for years 2001–2022. The IMERG data are re-gridded from their original 0.1°×0.1° spatial resolution onto the ERA5 grid. We used daily mean precipitation data.

Calculation of wet-bulb temperature

Daily mean Twb is calculated using daily mean dry-bulb temperature, dew-point temperature and surface pressure from ERA5. We used the method of Davies-Jones[45] with Python code made available by Raymond[46].

Identification of heatwaves

Humid heatwaves are identified daily for land areas between 35°S and 35°N during years 1993–2022:

- Hot humid days are identified separately in each grid cell. These are days when the daily mean Twb exceeds the 95th percentile for the local grid cell and exceeds a minimum threshold of 24°C. The 95th percentiles are calculated using daily data in each grid cell for all days during 1993–2022 and without using running means to avoid the pitfall highlighted by Brunner and Voigt[47].
- Hot humid days are aggregated into heatwave events using a 3-dimension connected components algorithm available in Python from https://pypi.org/project/connected-components-3d/[48].
- The heatwave events are filtered by imposing a minimum duration of 3 days in each grid cell, and a minimum spatial extent of 3 grid cells (~ 1900 km^2) throughout the lifetime of each heatwave.
- For consistency with the available GPM-IMERG data, heatwave data for years 2001–2022 is used in the analysis of the relationship between heatwaves and rainfall.
- We follow the practice of the World Meteorological Organization (WMO) and use a 30-year period (1993–2022) to calculate climatologies for heatwaves and other meteorological variables.

Identification of rainy days

To compare heatwaves with rainfall we categorised each day in 2001–2022 into two categories using precipitation data from GPM-IMERG. The category with higher rainfall (“High_Rain”) includes days when rainfall exceeds 5mm/day on that day, or the previous day, or on both days. The category with lower rainfall (“Low_Rain”) includes days when rainfall does not exceed 5mm/day on both that day and the previous day.

The empirical probability of heatwave occurrence for enhanced and suppressed rainfall days

For each grid cell we calculate the probability of heatwaves starting on High_Rain days:

$$\Pr\left(HW|High\_Rain\right) = \frac{N1}{N2}$$

1

where N1 is the number of High_Rain days on which a heatwave started, and N2 is the total number of High_Rain days. Similarly, we calculate the probability of heatwaves starting on Low_Rain days:

$$\Pr\left(HW|Low\_Rain\right) = \frac{N3}{N4}$$

2

where N3 is the number of Low_Rain days on which a heatwave started, and N4 is the total number of Low_Rain days.

The statistical significance of the difference between $\Pr\left(HW|High\_Rain\right)$ and $\Pr\left(HW|Low\_Rain\right)$ is tested following the method of Welty et al.[49]. We use a normal distribution approximation to the binomial test. The significance test is two-tailed and the significance level 5%.

The relative risk, sometimes referred to as the risk ratio, is calculated using one of two formulae:

$$Relative\ Risk = \frac{\Pr\left(HW|\ High\_Rain\right)}{\Pr\left(HW|\ Low\_Rain\right)}$$

3

or

$$Relative\ Risk = \frac{\Pr\left(HW|\ Low\_rain\right)}{\Pr\left(HW|\ High\_Rain\right)}$$

4

Equation (3) is used for grid cells where *Pr(HW|High_Rain)* is greater than *Pr(HW|Low_Rain)* and Eq. (4) is used where *Pr(HW|Low_Rain)* is greater than *Pr(HW|High_Rain)*. We use equations (3) and (4) for presentational purposes so that the relative risk varies over the same range of values (i.e. greater than 1) in all grid cells and all heatwave/rainfall regimes.

Ecosystem Limitation Index (ELI)

The ELI[33] is the difference between two correlation coefficients:

$$ELI = correlation\left(SLHF\prime, SM\prime\right) - correlation(SLHF\prime, SSRD\prime)$$

5

where SLHF’, SM’, and SSRD’ are anomalies from daily mean climatology for the surface latent heat flux, soil moisture, and surface SW radiation downwards. ELI is calculated daily using a 7-day moving window. We use daily anomalies and a 7-day window to capture variations in the surface environment on the time scale of humid heatwaves. We use a Spearman rank correlation to avoid assuming linear relationships.

The statistical significance of the heatwave composite ELI values was tested using the Wilcoxon signed rank test. This test was applied to the differences between $corr\,(SLHF\prime\,,SM\prime\,)$ and $corr(SLHF\prime\,,SSRD\prime\,)$ from values taken two days before each heatwave. Significance was determined at the 5% significance level.

Wet-bulb temperature limitation index (TwbLI)

The Twb limitation index (TwbLI) is motivated by the ELI[33]. The evapotranspiration term used by Denissen et al.[33] is replaced by Twb. TwbLI is the difference between two correlation coefficients:

$$TwbLI = correlation\,(Twb\prime\,,SM\prime\,) - correlation(Twb\prime\,,SSRD\prime\,)$$

6

where Twb’, SM’, and SSRD’ are anomalies from daily mean climatology for Twb, soil moisture, and surface SW radiation downwards. TwbLI is calculated daily using a 7-day moving window. We use a Spearman rank correlation.

The statistical significance of the heatwave composite TwbLI values was tested using the Wilcoxon signed rank test applied in the same way as for the ELI.

Declarations

Data availability

The ERA5 reanalysis data are available from the Copernicus Climate Change Service https://doi.org/10.24381/cds.adbb2d47 (single level data). GPM-IMERG data are available from https://catalog.data.gov/dataset/gpm-imerg-final-precipitation-l3-1-day-0-1-degree-x-0-1-degree-v07-gpm-3imergdf-at-ges-dis.

Code availability

Python 3 is used for data processing, analysis, and plotting. All custom codes use published implementations of standard methods and statistical techniques.

Acknowledgements

Funding was provided by NERC grant Humid heat extremes in the Global (sub)Tropics (H2X): NE/X013618/1 (Birch, Jackson, and Marsham) and NE/X013596/1 (Chagnaud and Taylor). We acknowledge the Copernicus Climate Change Service[50] for making available the ERA5 data[42,43] and the NASA Goddard Earth Sciences Data and Information Services Center for the GPM-IMERG data[44]. We gratefully acknowledge Colin Raymond and Rob Warren for making available Python code for calculating Twb[46] and William Silversmith for Python code for the connected components algorithm[48]. This work used JASMIN, the UK's collaborative data analysis environment (https://www.jasmin.ac.uk)[51].

Author contributions

Birch, Marsham, and Taylor designed the study. Jackson performed the analysis and wrote the first draft of the manuscript. Birch, Chagnaud, Marsham, and Taylor contributed to the interpretation of results and to writing of the final version of the manuscript.

Competing interests

The authors have no conflicts of interest to declare.

Additional information

References

1. Buzan J, R., Huber M (2020) Moist Heat Stress on a Hotter Earth. Annu Rev Earth Planet Sci 48:623–655. https://doi.org/10.1146/annurev-earth-053018-060100
2. Kjellstrom T et al (2016) Heat, Human Performance, and Occupational Health: A Key Issue for the Assessment of Global Climate Change Impacts. Annu Rev Public Health 37:97–112. https://doi.org/10.1146/annurev-publhealth-032315-021740
3. Sherwood SC, Huber M (2010) An adaptability limit to climate change due to heat stress. PNAS 107:21, 9552–9555. http://www.pnas.org/cgi/doi/ 10.1073/pnas.0913352107
4. Vecellio DJ, Kong Q, Kenney W, L., Huber M (2023) Greatly enhanced risk to humans as a consequence of empirically determined lower moist heat stress tolerance. PNAS 120:42, e2305427120. https://doi.org/10.1073/pnas.2305427120
5. Raymond C, Matthews T, Horton RM (2020) The emergence of heat and humidity too severe for human tolerance. Sci Adv 6:eaaw1838
6. Speizer S, Raymond C, Ivanovich C, Horton RM (2022) Concentrated and intensifying humid heat extremes in the IPCC AR6 regions. *Geophysical Research Letters* 49, e2021GL097261

https://doi.org/10.1029/2021GL097261

7. Rogers CDW et al (2021) Recent increases in exposure to extreme humid-heat events disproportionately affect populated regions. *Geophysical Research Letters* 48, e2021GL094183 https://doi.org/10.1029/2021GL094183
8. Powis CM et al (2023) Observational and model evidence together support widespread exposure to noncompensable heat under continued global warming. Sci Adv 9:36eadg9297. https://www.science.org/doi/ 10.1126/sciadv.adg9297
9. Zachariah M et al (2023) Extreme humid heat in South and Southeast Asia in April 2023, largely driven by climate change, detrimental to vulnerable and disadvantaged communities. https://doi.org/10.25561/104092
10. Russo S, Sillmann J, Sterl A (2017) Humid heat waves at different warming levels. Sci Rep 7:7477. 10.1038/s41598-017-07536-7
11. Coffel ED, Horton RM, de Sherbinin A (2018) Temperature and humidity based projections of a rapid rise in global heat stress exposure during the 21st century. Environ Res Lett 13:014001. https://doi.org/10.1088/1748-9326/aaa00e
12. Li D, Yuan J, Kopp RE (2020) Escalating global exposure to compound heat-humidity extremes with warming. Environ Res Lett 15:064003. https://doi.org/10.1088/1748-9326/ab7d04
13. Parkes B, Buzan JR, Huber M (2022) Heat stress in Africa under high intensity climate change. Int J Biometeorol 66:1531–1545. https://doi.org/10.1007/s00484-022-02295-1
14. Safieddine S, Clerbaux C, Clarisse L, Whitburn S, Eltahir EAB (2022) Present and future land surface and wet bulb temperatures in the Arabian Peninsula. Environ Res Lett 17:044029. https://doi.org/10.1088/1748-9326/ac507c
15. Zeppetello LRV, Raftery AE, Battisti DS (2022) Probabilistic projections of increased heat stress driven by climate change. Commun Earth Environ 3:183. https://doi.org/10.1038/s43247-022-00524-4
16. Domeisen DIV et al (2023) Prediction and projection of heatwaves. Nat reviews earth Environ 4:36–50. https://doi.org/10.1038/s43017-022-00371-z
17. Raymond C et al (2021) On the controlling factors for globally extreme humid heat. *Geophysical Research Letters* 48, e2021GL096082 https://doi.org/10.1029/2021GL096082
18. Birch CE et al (2022) Future changes in African heatwaves and their drivers at the convective scale. *Journal of Climate* 35, 5981–6006 doi10.1175/JCLI-D-21-0790.1
19. Ivanovich CC, Horton RM, Sobel AH, Singh D (2024) Subseasonal variability of humid heat during the South Asian summer monsoon. *Geophysical Research Letters* 51, e2023GL107382 https://doi.org/10.1029/2023GL107382
20. Zhang Z et al (2024) Light rain exacerbates extreme humid heat. Nat Commun 15:7326. https://doi.org/10.1038/s41467-024-51778-9

21. Mishra V et al (2020) Moist heat stress extremes in India enhanced by irrigation. Nat Geosci 13:722–728. https://doi.org/10.1038/s41561-020-00650-8
22. Kang S, Eltahir E (2018) North China Plain threatened by deadly heatwaves due to climate change and irrigation. Nat Commun 9:2894. 10.1038/s41467-018-05252-y
23. Jha R, Mondal A, Devanand A, Roxy MK, Ghosh S (2022) Limited influence of irrigation on pre-monsoon heat stress in the Indo-Gangetic Plain. Nat Commun 13:4275. https://doi.org/10.1038/s41467-022-31962-5
24. Simpson CH, Brousse O, Ebi KL, Heaviside C (2023) Commonly used indices disagree about the effect of moisture on heat stress. Clim Atmospheric Sci 6:78. https://doi.org/10.1038/s41612-023-00408-0
25. Krakauer NY, Cook BI, Puma MJ (2020) Effect of irrigation on humid heat extremes. Environ Res Lett 15:094010. https://doi.org/10.1088/1748-9326/ab9ecf
26. Miralles DG, Gentine P, Seneviratne SI, Teuling AJ (2018) Land–atmospheric feedbacks during droughts and heatwaves: state of the science and current challenges. Ann N Y Acad Sci 1436:19–35. 10.1111/nyas.13912
27. Denissen JMC et al (2024) Intensified future heat extremes linked with increasing ecosystem water limitation. Earth Syst Dynam 15:717–734. https://doi.org/10.5194/esd-15-717-2024
28. Kong Q, Huber M (2023) Explicit calculations of wet-bulb globe temperature compared with approximations and why it matters for labor productivity. Earths Future 10. https://doi.org/10.1029/2021EF002334. e2021EF002334
29. Seneviratne S (2010) Investigating soil moisture–climate interactions in a changing climate: A review. Earth Sci Rev 99:125–161. http://dx.doi.org/10.1016/j.earscirev.2010.02.004
30. Hirsch AL et al (2019) Amplification of Australian heatwaves via local land-atmosphere coupling. J Geophys Res Atmos 124:13,625–13647. https://doi.org/10.1029/2019JD030665
31. Vogel MM, Zscheischler J, Fischer EM, Seneviratne SI (2020) Development of future heatwaves for different hazard thresholds. *Journal of Geophysical Research Atmospheres* 125, e2019JD032070 https://doi.org/10.1029/2019JD032070
32. Lo S-H, Chen C-T, Russo S, Huang G-R, Shih M-F (2021) Tracking heatwave extremes from an event perspective. Weather Clim Extremes 34:100371. https://doi.org/10.1016/j.wace.2021.100371
33. Denissen JMC et al (2022) Widespread shift from ecosystem energy to water limitation with climate change. Nat Clim Change 12:677–684. https://doi.org/10.1038/s41558-022-01403-8
34. Zhang Y, Held I, Fueglistaler S (2021) Projections of tropical heat stress constrained by atmospheric dynamics. Nat Geosci 14:133–137. https://doi.org/10.1038/s41561-021-00695-3
35. Justine J, Monteiro JM, Shah H, Rao N (2023) The diurnal variation of wet bulb temperatures and exceedance of physiological thresholds relevant to human health in South Asia. Commun Earth Environ 4:244. https://doi.org/10.1038/s43247-023-00897-0

36. Beck HE et al (2018) Present and future Köppen-Geiger climate classification maps at 1-km resolution. Sci Data 5:180214. 10.1038/sdata.2018.214
37. National Weather Service https://www.weather.gov/safety/heat-index
38. Zhang W, Villarini G (2020) Deadly Compound Heat Stress-Flooding Hazard Across the Central United States. *Geophysical Research Letters* 47, e2020GL089185 https://doi.org/10.1029/2020GL089185
39. Li M, Gu S, Bi P, Yang J, Liu Q (2015) Heat Waves and Morbidity: Current Knowledge and Further Direction - A Comprehensive Literature Review. Int J Environ Res Public Health 12:5, 5256–5283. 10.3390/ijerph120505256
40. Sherwood SC (2018) How Important Is Humidity in Heat Stress? J Geophys Research: Atmos 123:11, 808–11810. https://doi.org/10.1029/2018JD028969
41. Seneviratne SI et al (2021) Weather and Climate Extreme Events in a Changing Climate. Climate Change 2021: The Physical Science Basis. Contribution of Working Group I to the Sixth Assessment Report of the Intergovernmental Panel on Climate Change. Cambridge University Press, Cambridge, United Kingdom and New York, NY, USA, pp 1513–1766. doi: 10.1017/9781009157896.013
42. Hersbach H et al (2023) ERA5 hourly data on single levels from 1940 to present. Copernicus Climate Change Service (C3S) Climate Data Store (CDS). Accessed July-December 2023. 10.24381/cds.adbb2d47
43. Hersbach H et al (2023) ERA5 hourly data on pressure levels from 1940 to present. Copernicus Climate Change Service (C3S) Climate Data Store (CDS). Accessed July-December 2023. 10.24381/cds.bd0915c6
44. Huffman GJ, Stocker EF, Bolvin DT, Nelkin EJ (2019) & Jackson Tan. GPM IMERG Final Precipitation L3 1 day 0.1 degree x 0.1 degree V06, Edited by Andrey Savtchenko, Greenbelt, MD, Goddard Earth Sciences Data and Information Services Center (GES DISC), Accessed December 2023 to January 2024, 10.5067/GPM/IMERGDF/DAY/07
45. Davies-Jones R (2008) An efficient and accurate method for computing the wet-bulb temperature along pseudoadiabats. Mon Weather Rev 136:7, 2764–2785. 10.1175/2007MWR2224.1
46. Raymond C (2023) October. https://github.com/cr2630git/wetbulb_dj08_spedup, accessed 16
47. Brunner L, Voigt A (2087) Pitfalls in diagnosing temperature extremes. *Nat Commun* 15, https://doi.org/10.1038/s41467-024-46349-x (2024)
48. Silversmith W connected-components-3d-3.12.1, https://pypi.org/project/connected-components-3d/, downloaded 15 January 2024.
49. Welty J, Stillman S, Zeng X, Santanello J (2020) Increased likelihood of appreciable afternoon rainfall over wetter or drier soils dependent upon atmospheric dynamic influence. *Geophysical Research Letters* 47, e2020GL087779 https://doi.org/10.1029/2020GL087779
50. Copernicus Climate Change Service (2023) : ERA5 hourly data on single levels from 1940 to present. Copernicus Climate Change Service (C3S) Climate Data Store (CDS), https://doi.org/10.24381/cds.adbb2d47 (Accessed July-December 2023)

51. Lawrence BN et al (2013) Storing and manipulating environmental big data with JASMIN. In: IEEE Big Data, October 6–9, San Francisco, (2013)

Figures

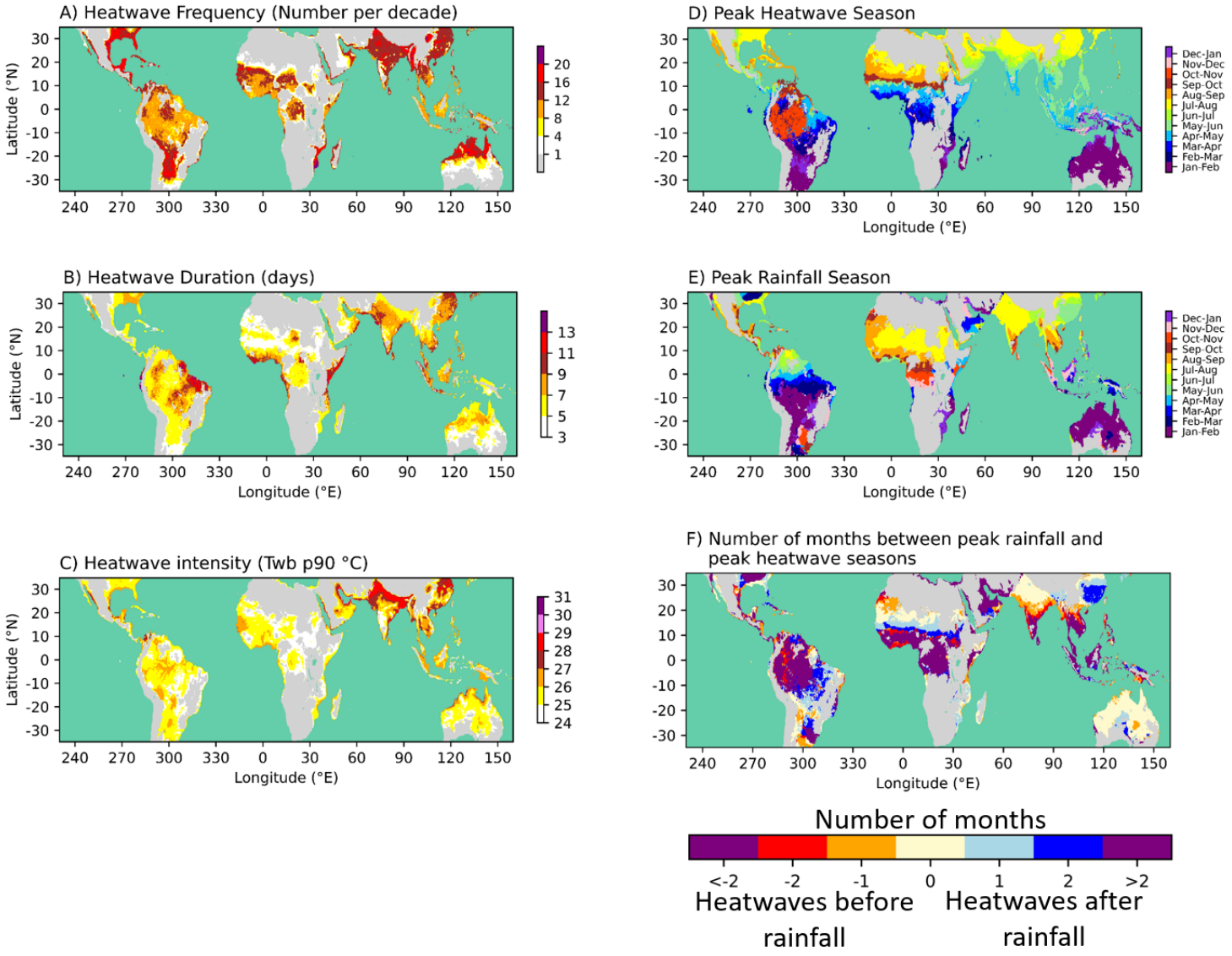

Figure 1

Humid heatwaves over land in the global tropics and subtropics, and the seasonality of rainfall and humid heatwaves. A) The frequency of heatwaves in each grid cell expressed as the number per decade. B) The mean duration of heatwaves in each grid cell. C) Heatwave intensity in each grid cell, represented by the 90th percentile (p90) of daily mean Twb on heatwave days. D) The two-month period during a calendar year in which most heatwaves occur. E) The two-month period during a calendar year in which the highest rainfall occurs in GPM-IMERG (2001 to 2022). F) The number of months between the month

of peak rainfall and the month of peak heatwave occurrence. Regions with no heatwaves are shaded grey.

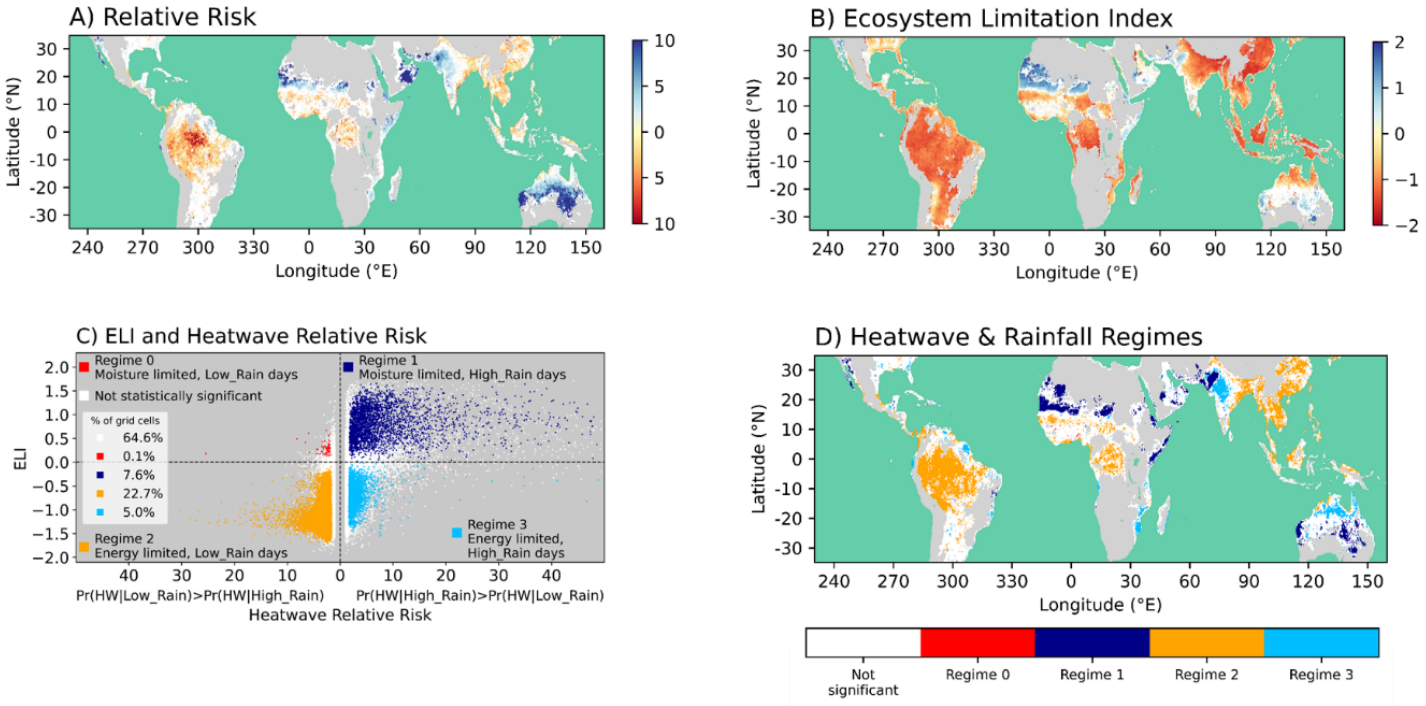

Figure 2

Linking the occurrence of heatwaves to rainfall (2001-2022). A) Relative risk of heatwave occurrence on High_Rain (blue) and Low_Rain (red) days. B) The Ecosystem Limitation Index: moisture-limited regions (ELI > 0), energy-limited regions (ELI < 0). C) Scatter plot of ELI against relative risk and the percentage of grid cells in each regime (inset). D) Map of the heatwave and rainfall regimes defined in panel C). In panels A, B, and D, no humid heatwaves were identified in regions shaded grey. In all panels, regions not significant at the 5% level are shaded white.

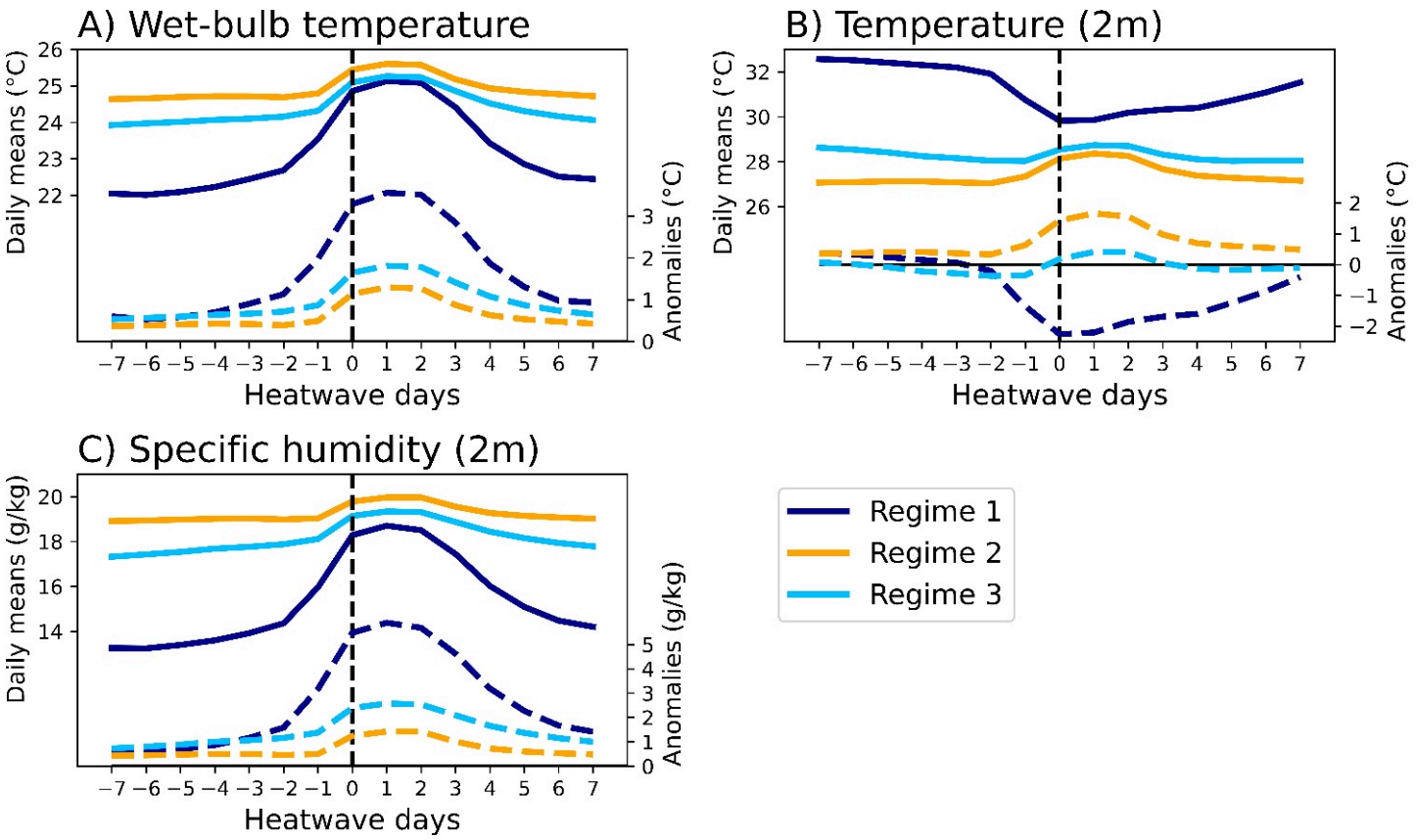

Figure 3

Heatwave composite time series for: A) Twb, B) temperature (2m), and C) specific humidity (2m). The time series run from 7 days before the start of each heatwave (day -7) to 7 days after the start of each heatwave (day 7). Day 0 is the heatwave start day. Solid lines and the y-axis on the left of each panel show composite daily mean values. Dashed lines and the y-axis on the right show composite anomalies from the local 1993-2022 daily mean climatology.

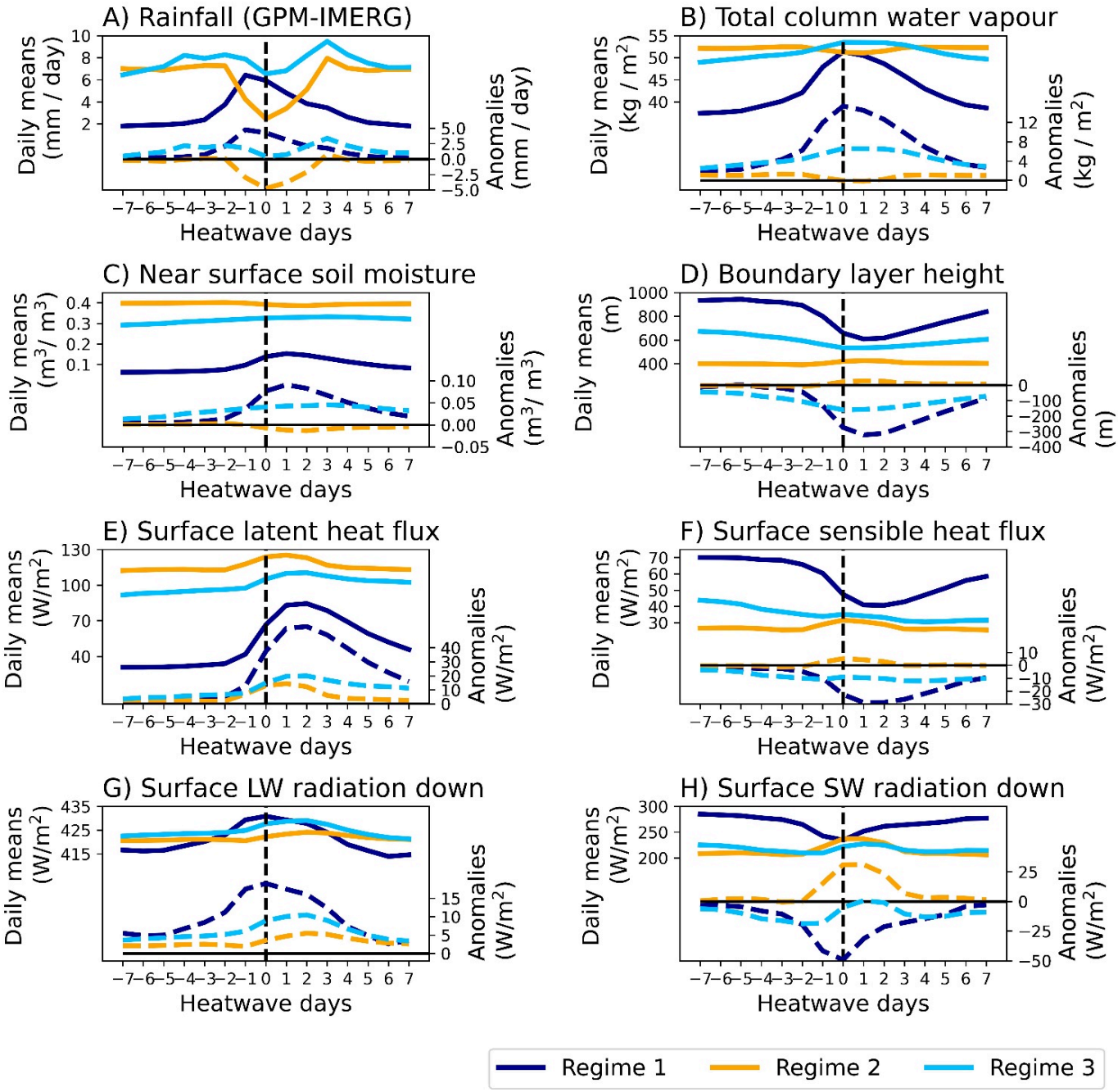

Figure 4

Heatwave composite time series from 7 days before the start of each heatwave (day -7) to 7 days after the start of each heatwave (day 7). Day 0 is the heatwave start day. Solid lines and the y-axis on the left of each panel show daily mean values. Dashed lines and the y-axis on the right show anomalies from the local 1993-2022 daily mean climatology.

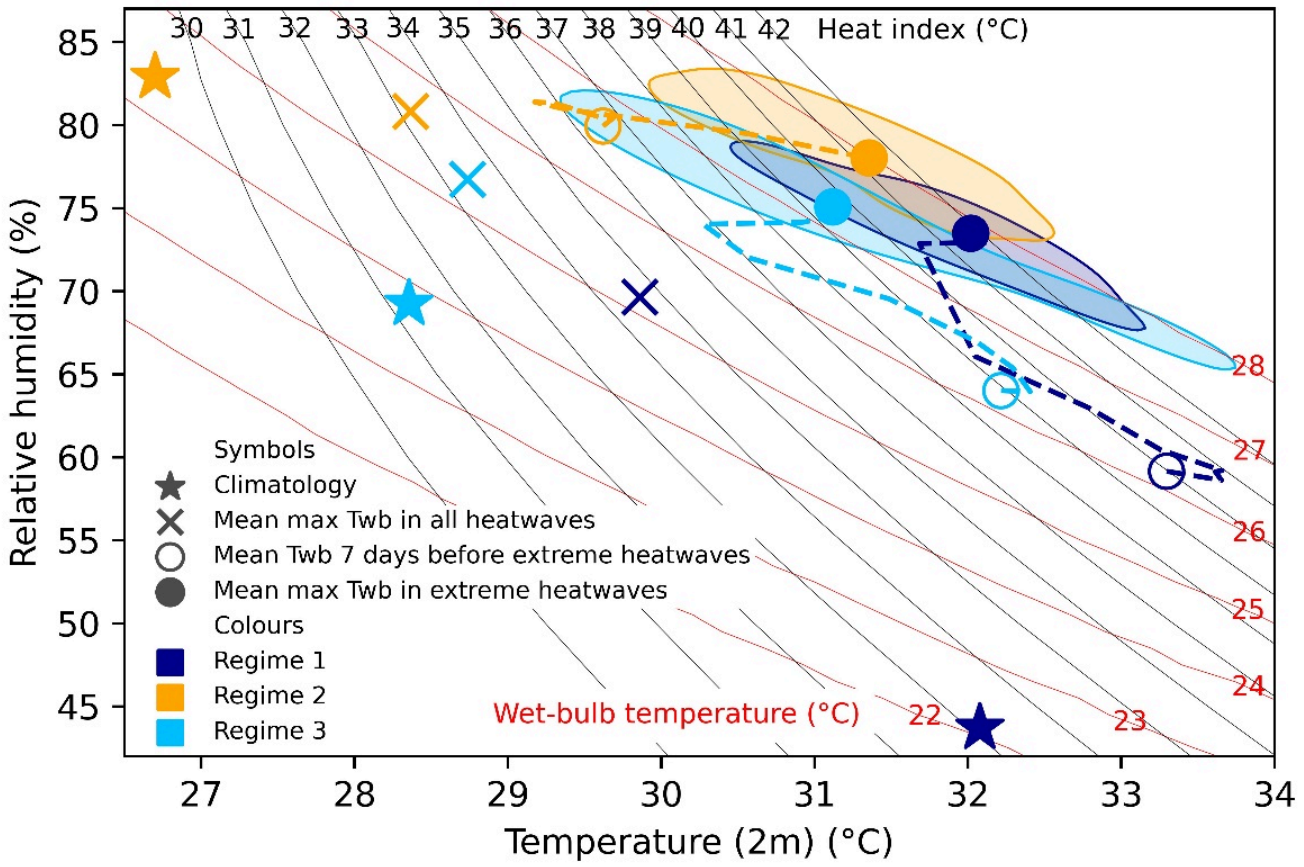

Figure 5

Climatology (1993-2022) and humid heatwave conditions in each regime plotted on isopleths of Twb and Heat Index. The dashed lines show the daily time series from day -7 (open circle) to day +2 (solid circle) for the most extreme heatwaves (events with 10% highest Twb). The shaded areas show the distribution of temperature and humidity on the 2nd day of the extreme heatwaves. The shaded areas contain 50% of the extreme heatwave grid cells and their boundary contour presents the 50th percentile. Extreme heatwaves are the heatwaves in each grid cell that have the highest 10% of Twb.

Supplementary Files

This is a list of supplementary files associated with this preprint. Click to download.

- SupplementaryinformationNatCommssubmitted.docx